Applied Physics Letters

RESEARCH ARTICLE | NOVEMBER 03 2022

Near-room temperature topological Hall effect at spin reorientations in sputtered $NdCo_{5-x}Cu_x$ thin film

Satoshi Sugimoto ; Yukiko K. Takahashi ; Shinya Kasai

Appl. Phys. Lett. 121, 182404 (2022)
https://doi.org/10.1063/5.0128572

Articles You May Be Interested In

Tunability of the spin reorientation transitions with pressure in $NdCo_5$

Appl. Phys. Lett. (March 2020)

Crystal structure, spin reorientation, and rotating magnetocaloric properties of $NdCo_{5-x}Si_x$ compounds

J. Appl. Phys. (June 2019)

Spin reorientation in $NdCo_5$ single crystals

AIP Conference Proceedings (May 1976)

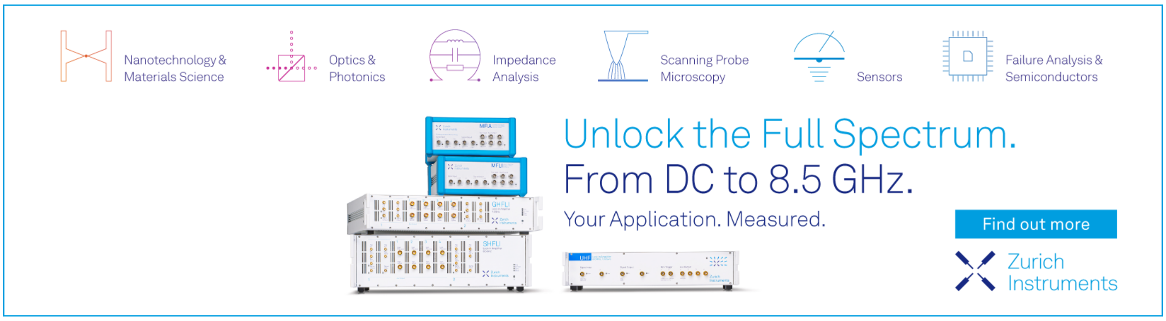

AIP Publishing

Applied Physics Letters ARTICLE scitation.org/journal/apl

Near-room temperature topological Hall effect at spin reorientations in sputtered $NdCo_{5-x}Cu_x$ thin film

Cite as: Appl. Phys. Lett. **121**, 182404 (2022); doi: 10.1063/5.0128572
Submitted: 29 September 2022 · Accepted: 17 October 2022 ·
Published Online: 3 November 2022

Satoshi Sugimoto,[a] Yukiko K. Takahashi, and Shinya Kasai

AFFILIATIONS

Research Center for Magnetic and Spintronic Materials, National Institute for Materials Science (NIMS), 1-2-1 Sengen, Tsukuba 305-0047, Japan

[a] Author to whom correspondence should be addressed: SUGIMOTO.Satoshi@nims.go.jp

ABSTRACT

The spin reorientation in rare-earth intermetallics involves distinctive magnetic morphologies commencing with spontaneous skyrmion textures without an external magnetic field. Here, we present the sputtering growth of $CaCu_5$-type $NdCo_{5-x}Cu_x$ thin films on MgO (110) substrates. Our films exhibit two successive spin reorientation transitions between the *ab*-plane and the *c*-axis, close to the room temperature, apart from the non-uniaxial behavior below 150 K. The corresponding modulations of magnetocrystalline anisotropy at reorientation temperatures lead to the large topological Hall effect, which can be maintained up to 250 K with a maximum Hall resistivity of 210 nΩ cm. These results of robust topological signals will provide platforms for realizing room-temperature topological magnetic textures.

The Berry curvature of topological magnetic textures results in the distinctive transverse Hall current stemming from the interaction of the magnetic order and intrinsic band structure or scattering.[1] The intrinsic anomalous Hall effect (AHE)[2–5] and the topological Hall effect (THE)[6,7] are two physical phenomena routed to such topological origins. THE is driven by the pseudo magnetic field emerging in the magnetic domains. It is commonly considered as a benchmark for the existence of topological and/or nonlinear magnetic textures[8,9] such as skyrmions. Magnetic skyrmions are nanometric bubble domains with a unit integer topological charge, anticipated as a generation of high density, high speed, and low energy consumption information storage units.[10] Room-temperature, zero magnetic field stabilizing skyrmions are particularly favorable for applications in future devices, owing to their reduced complication and energy consumption.[11] Nonetheless, ground-state stripe domains in most chiral ferromagnetic materials with Dzyaloshinskii–Moriya interactions (DMIs)[12–15] inhibit the stabilization of the skyrmion texture in the absence of a magnetic field and/or extrinsic factors.[16–19]

However, recent results have been reported by Zuo *et al.* demonstrating direct imaging of spontaneous skyrmion type textures in the absence of an external field over a wide range of temperatures up to 280 K in rare-earth $NdCo_5$ alloys.[20] These key observations have been attributed to two successive spin reorientation transitions (SRTs) near room temperature, known as (1) the "easy-plane" to "easy-cone" transition at $T_{SR1} \sim 240$ K and (2) the easy-cone to "easy-axis" transition at $T_{SR2} \sim 280$ K.[21,22] The associated underlying physical principle has been primarily developed by Moon *et al.*[23] They have proposed that the perpendicular magnetic anisotropy (PMA) to the in-plane-magnetic-anisotropy (IMA) transition at SRTs can maintain the perpendicular magnetization under very weak DMI, resulting in the formation of spontaneous skyrmion textures in the in-plane-magnetization system. Such characteristic SRTs are widely observed for rare earth-cobalt intermetallics arising from the competing magnetic anisotropies of the rare earth sublattice and the Co sublattice. Thus, the recent discovery of spontaneous skyrmions in $NdCo_5$ has motivated the exploration of various topological spin textures in rare-earth intermetallics.

Nevertheless, in spite of the unique characteristics related to SRTs, thin film engineering of $NdCo_5$ intermetallics has remained scarcely explored thus far. Following the early studies of Sm- or Nd-included rare-earth intermetallics,[24,25] high-energy sputtering techniques have been commonly employed for the sole fabrication of amorphous $NdCo_5$ solids, which generally exhibit strong PMA but weak SRT natures.[26,27] Bulk SRT characteristics have been observed for epitaxial $NdCo_5$ thin films by Seifert *et al.* using the pulsed laser deposition (PLD) technique.[28,29] However, investigations of topological magnetic domains and related physics have been barely reported so far.

In this Letter, we present the development of a magnetron sputtering technique for the fabrication of $NdCo_5$ intermetallics, which reproduce distinctive SRTs of bulk nature. The presence of a topological Hall effect (THE) associated with SRTs is demonstrated throughout magneto-transport measurements. Fractional substitutions of Co sites by Cu atoms in $CaCu_5$-type $NdCo_5$ are adopted to improve the crystallinity of thin film samples, enabling robust THE maintained at a wide temperature range. We further observe non-uniaxial magnetocrystalline anisotropy (MCA) at lower temperature, where additional Hall signals phenomenologically increase due to the shape effect of thin films.

$NdCo_{5-x}Cu_x$ thin films (10–50 nm) were grown on MgO (110) substrates with a 10 nm thick Cr buffer layer using dc magnetron co-sputtering from Nd, Co, and Cu targets. The MgO substrates were annealed at 600 °C for 1 h, and a Cr buffer was sputtered on the surface at 400 °C. Subsequently, $NdCo_{5-x}Cu_x$ films were sputtered at 600–800 °C prior to adding a capping layer of 5 nm thick Ta. Stoichiometry of the resulting $NdCo_{5-x}Cu_x$ films was evaluated as $x = 0.0$, 0.6, 1.3, and 2.0 using x-ray fluorescence analysis (XRF, Rigaku). The crystal structures of the $NdCo_{5-x}Cu_x$ films were characterized using x-ray diffraction (XRD, Rigaku) with a Cu-Kα source ($\lambda = 1.5406$ Å). Magnetization measurements were performed by a vibrating sample magnetometry technique using a magnetic property measurement system (MPMS, Quantum Design). The transport properties were measured for the 20–40 μm width Hall bars by a four-probe method using a physical property measurement system (PPMS, Quantum Design).

The $NdCo_5$ hexagonal crystal forms a $CaCu_5$-type structure, classified in the space group P6/mmm, no. 191. The XRD profiles of $NdCo_{5-x}Cu_x$ films shown in Fig. 1(a) confirm the formation of an Nd-Co phase with an orientation of the *c*-axis parallel to the MgO (001) direction in agreement with former studies of PLD deposited $NdCo_5$ systems.[28] Sharpe $NdCo_5$ $(10\bar{1}0)$ and $(20\bar{2}0)$ peaks are observed at 2θ positions of 20.8° and 42.7° for Cu-free $NdCo_5$ sputtered films onto the crystallized Cr buffer layer along the (211) orientation. The texture relation is summarized as $NdCo_5(10\bar{1}0)[0001] \parallel Cr(211)[0\bar{1}1] \parallel MgO(110)[001]$.

By increasing the Cu content in the $NdCo_{5-x}Cu_x$ films from $x = 0.0$ to $x = 2.0$, a decrease in the width of the $(10\bar{1}0)$ and $(20\bar{2}0)$ peaks is observed, accompanied by the emergence of the $(30\bar{3}0)$ and $(40\bar{4}0)$ higher peaks at $2\theta = 63.7°$ and 89.5°. This reveals a notable improvement in the crystallinity of sputtered films by substituting Co sites with small amounts of Cu. The FWHM of a rocking curve of ω-scans at $(20\bar{2}0)$ peaks for different Cu contents is plotted in Fig. 1(b). The width decreases linearly with increasing Cu content for lower temperature sputtering at 600 °C. For higher temperature sputtering at 800 °C, the FWHM notably decreases from $x = 0.0$ to $x = 0.4$, and it reaches to $\Delta\omega < 1°$ for higher Cu contents. Such distinctive improvement of the sputtered films can be attributed to the high solubility of Cu atoms in the $CaCu_5$-type crystal, which has been discovered earlier.[30] Note that Cu substitutions also affect MCA assigned to a decrease in the net magnetic moment at each Cu site. The *c*-axis MCA constant *K* for lower temperature sputtering is plotted in Fig. 1(b). MCA shows a monotonic decrease with increasing Cu contents, indicating higher Cu substitution will degrade the original magnetic properties of the $CaCu_5$-type $NdCo_5$ crystal. For balancing the high crystallinity and large MCA, we would focus on $NdCo_{4.4}Cu_{0.6}$ ($x = 0.6$) samples for subsequent discussions.

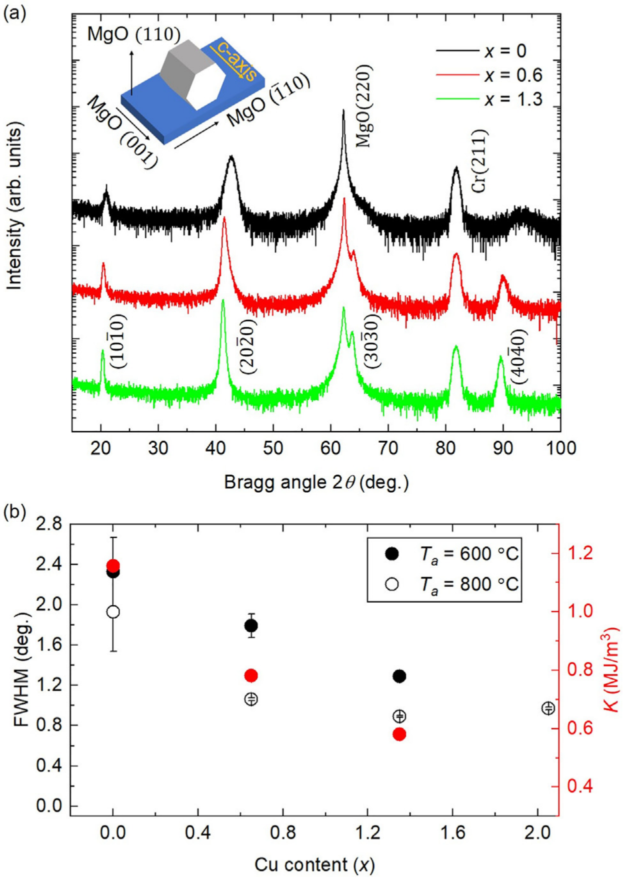

FIG. 1. Structural characterization of the $NdCo_{5-x}Cu_x$ sputtered thin films. (a) X-ray diffraction patterns of a 25 nm $NdCo_{5-x}Cu_x$ thin film. Different Cu contents with $x = 0$, 0.6, and 1.3 are plotted with black, red, and green colors, respectively. The texture relation with the MgO substrate is depicted in the inset. (b) The full width at half maximum of the NdCo5 $(20\bar{2}0)$ peak (black open and closed symbols) and the *c*-axis magnetocrystalline anisotropy constant *K* (red symbols) for different Cu contents. Values of *K* are investigated for 600 °C annealed films at 400 °C.

The temperature dependencies of the magnetization process for $NdCo_{4.4}Cu_{0.6}$ thin films are presented in Fig. 2(a). The zero-field cooling process exhibits an abrupt decrease in the magnetization along the *c*-axis around $T = 275$ K, reflecting to the easy-axis to easy-cone transition labeled as T_{SR2}. The magnetization is completely diminished around $T = 230$ K, which corresponds to the rotation of the easy axis to the *ab*-plane, referred to as the easy-cone to easy-plane transition at T_{SR1}. These successive reorientation processes are also observed at the same temperatures for the zero-field heating process. This indicates that SRTs, unique to $CaCu_5$-type $NdCo_5$, are plausibly reproduced for our sputtered thin films. It is worth noting that these SRTs, observed in our texture relation, correspond to the PMA to IMA transition applicable for spontaneous skyrmions formations.[20,23]

Further details regarding the magnetization process related to SRTs can be discussed from the hysteresis loops along the three

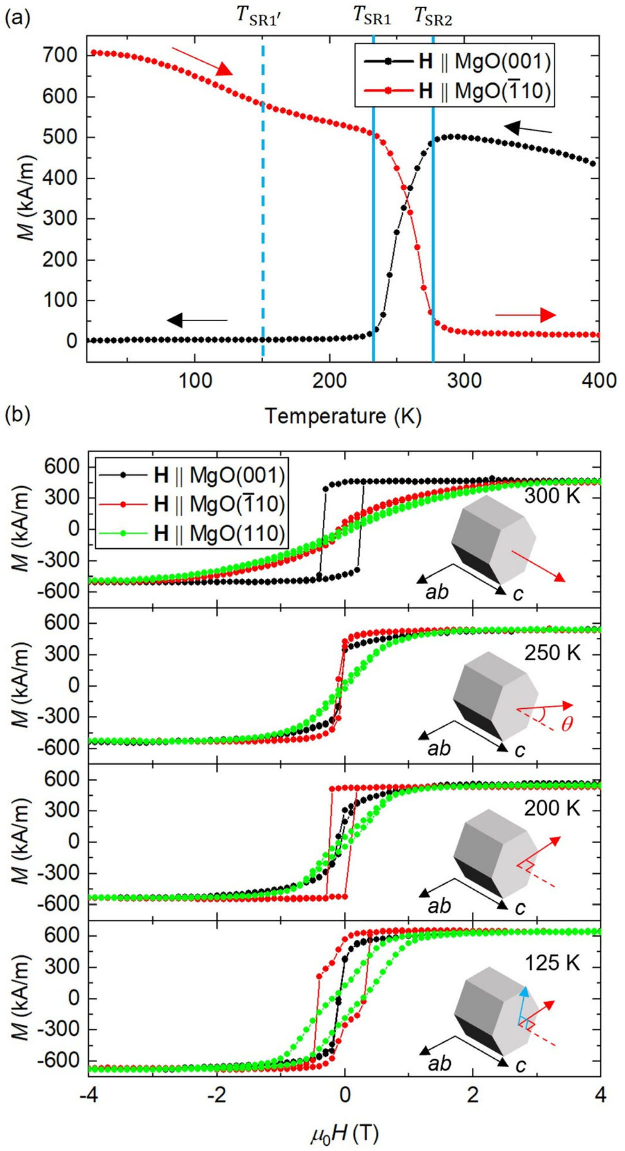

FIG. 2. Magnetic property of 25 nm thick $NdCo_{4.4}Cu_{0.6}$ films. (a) Temperature dependencies of the magnetic moment M for the zero-field cooling (black) and the zero-field heating (red) processes. The sample magnetization is once saturated by an external 6 T field along the MgO (001) (cooling) or ($\bar{1}$10) (heating) directions. (b) Hysteresis loops along the MgO (001) (black), ($\bar{1}$10) (red), and (110) (green) directions for the easy-axis phase ($T = 300$ K, top), easy-cone phase (250 K, second), easy-plane phase (200 K, third), and biaxial *ab*-plane phase (125 K, bottom). Schematics of the MCA axis at each phase are depicted in the insets.

crystalline orientations shown in Fig. 2(b). For the easy-axis phase at 300 K, the square-shaped hysteresis loop is obtained only along the MgO (001) direction. Meanwhile, the hard-axis behaviors are observed along the MgO ($\bar{1}$10) and (110) directions, indicating that the uniaxial MCA axis is along the *c*-axis. At 250 K, the square hysteresis is once diminished, and soft magnetization loops along the MgO (001) and ($\bar{1}$10) directions are obtained. These results reproduce the easy-cone phase, where the MCA axis is intermediately tilted from the *c*-axis direction toward the *ab*-plane. Note that only the magnetization process along the MgO (110) direction shows the strong hard-axis behavior due to the large demagnetization field characteristic of nanometer-scale thickness films. For the easy-plane phase at 200 K, the easy-axis hysteresis is obtained along the MgO ($\bar{1}$10) direction, showing a rotation of the MCA axis from the *c*-axis direction to the *ab*-plane. These three distinctive MCA rotations are inherited in $CaCu_5$-type $NdCo_5$.

Meanwhile, the unique hysteretic behaviors start to appear once the temperature decreases below 150 K. At 125 K, the magnetization processes along both MgO ($\bar{1}$10) and (110) directions exhibit step-like hysteretic behaviors. These results can be regarded as the "biaxial *ab*-plane" MCA rather than a simple "uniaxial" MCA rotation unique to $CaCu_5$-type $NdCo_5$. Such a complex MCA is considered in association with the enhanced PMA component at low temperatures and/or effects of the mixed crystal with the Nd-rich solids as discussed in Fig. 4. Stabilizations of multi-domains and/or nonlinear magnetic textures within the *ab*-plane are conceivable from the hysteresis shapes at this temperature range. The sign of this additional "biaxial" phase is also observed as a small kink at $T \sim 150$ K at the zero-field heating curve, labeled as $T_{SR1'}$ where magnetization exhibits a slight increase from the easy-plane phase. These three distinctive SRTs also affect longitudinal and transport properties in Figs. 3(a) and 3(b). The two tiny kinks appear around 260 and 160 K. The former allocates between T_{SR2} and T_{SR1}, and the latter lies in the vicinity of $T_{SR1'}$ corresponding to SRT temperatures in Fig. 2(a).

Magneto-transport properties in $NdCo_{4.4}Cu_{0.6}$ sputtered films are discussed by measuring the Hall resistivity at each reorientation phase. The total Hall resistivity ρ_{xy} can be described from contributions of the ordinary Hall effect (OHE), AHE, and THE, as $\rho_{xy} = \rho_{xy}^{\mathrm{OHE}} + \rho_{xy}^{\mathrm{AHE}} + \rho_{xy}^{\mathrm{THE}}$. The resistivity of OHE is linearly proportional to the external field H, described as $\rho_{xy}^{\mathrm{OHE}} = R_0 H$, with a Hall coefficient R_0. The modern understanding of AHE includes intrinsic and side-jump scattering contributions.[1,31] Thus, the resistivity could be expressed as $\rho_{xy}^{\mathrm{AHE}} \sim S_A \rho_{xx}^2 M$ using a scaling coefficient S_A, longitudinal resistivity ρ_{xx}, and the magnetization M. The remaining resistivity of THE can be simplified as follows:

$$\rho_{xy}^{\mathrm{THE}} = \rho_{xy} - R_0 H - S_A \rho_{xx}^2 M.$$

Figure 4 exhibits the field dependencies of ρ_{xy}, $\rho_{xy}^{\mathrm{OHE}} + \rho_{xy}^{\mathrm{AHE}}$, and ρ_{xy}^{THE} for a 25 nm thick $NdCo_{4.4}Cu_{0.6}$ sample at different reorientation phases, as the easy-axis ($T = 300$ K), easy-cone (250 K), easy-plane (200 K), and biaxial *ab*-plane phases below $T_{SR1'}$ (125 K). The values of R_0 and R_S are estimated at the uniformly saturated condition under $H = 4$ T. When the $NdCo_{4.4}Cu_{0.6}$ film shows an easy-axis MCA at 300 K, the difference between $\rho_{xy}(H)$ and $\rho_{xy}^{\mathrm{OHE}}(H) + \rho_{xy}^{\mathrm{AHE}}(H)$ curve is almost negligible. This indicates the negligible topological contribution onto magnetization here. Once the temperature decreases below T_{SR2} to 250 K, the $NdCo_{4.4}Cu_{0.6}$ film shifts to an easy-cone phase, as confirmed in Fig. 2(a), and the PMA to IMA transition affects the underlying magnetic textures. As expected, the $\rho_{xy}(H)$ curve shows a clear difference from $\rho_{xy}^{\mathrm{OHE}}(H) + \rho_{xy}^{\mathrm{AHE}}(H)$ at zero-field vicinity $|H| < 1$ T, and an apparent nonzero topological contribution is detected. ρ_{xy}^{THE} shows a symmetric behavior against zero field and is maximized at $H = \pm 0.3$ T up to $\rho_{xy}^{\mathrm{THE}}|_{\max} \sim 88$ nΩ cm. The obtained topological signal scale and its external field evolution show a good

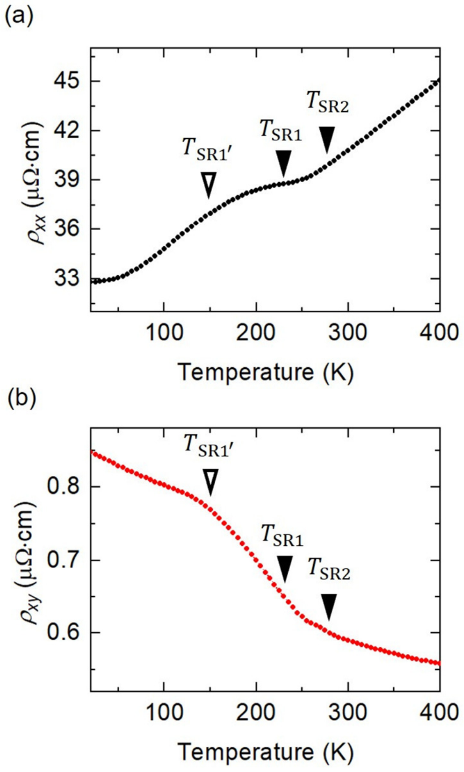

FIG. 3. Temperature dependence of the (a) longitudinal resistivity ρ_{xx} and (b) transverse resistivity ρ_{xy} of 25 nm thick $NdCo_{4.4}Cu_{0.6}$ films. The spin reorientation temperatures $T_{SR1'}$, T_{SR1}, and T_{SR2} obtained from Fig. 2 are marked by closed or open triangles.

consistency with direct imaging results by TEM observations reported in Ref. 20. According to this report, the spontaneous enclosed in-plane domains (EIPDs) and stripe domains are stabilized as magnetic ground states in the absence of an external field. These domains transform into biskyrmions[32] under a small field range of 0.2–0.3 T, leading to a finite THE. Under a higher external field, such biskyrmions are swept away, resulting in a "hump-like" shape in the THE field dependencies observed in Fig. 4. The emergence of such a distinctive topological Hall signal is also observed for the easy-plane phase at 200 K, where the maximum signal amplitude and the peak field positions remain almost constant from the easy-cone phase at 250 K. These results imply that EIPDs and/or biskyrmions are stabilized in the wide temperature range from easy-cone to easy-plane phases ($150\,K < T \leq 250\,K$).

At a further low temperature (125 K), the biaxial MCA behavior results in an increment of the topological contribution up to $\rho_{xy}^{THE}|_{max}$ $\sim$162 nΩ cm at the peak positions of $H = \pm 0.5\,T$. In addition, ρ_{xy}^{THE} curves indicate small hysteretic behaviors between the different field sweep directions. These lower temperature characteristics are unique to thin film samples, implying a stabilization of other types of nonlinear magnetic textures. As is apparent in results of 125 K in Fig. 2(b), thin film samples exhibit a finite PMA component involved for stabilizing conventional PMA skyrmions[33,34] and/or magnetic vortices.[35] PMA skyrmions and/or vortices possess constant topological charges at zero-field vicinity, resulting in unique two-block shapes in their hysteresis loops.[35–37] The quenched-shaped magnetization curve at 125 K (approximated by $\rho_{xy}^{OHE} + \rho_{xy}^{AHE}$) in Fig. 4 shows certain analogies with a feature of such two-block shape hysteresis loops, inferring stabilization of these chiral magnetic textures. On the other hand, it is difficult to exclude multicarrier effects attributed to the non-$CaCu_5$-type Nd intermetallics. Nd-rich Ce_2Ni_7-type Nd_2Co_7 shows good lattice matches with $CaCu_5$-type $NdCo_5$ in hexagonal lattice constant $a = b = 5.02$ Å with $c = 4.06$ Å ($NdCo_5$) and $c = 24.36$ Å (Nd_2Co_7)[28,38]

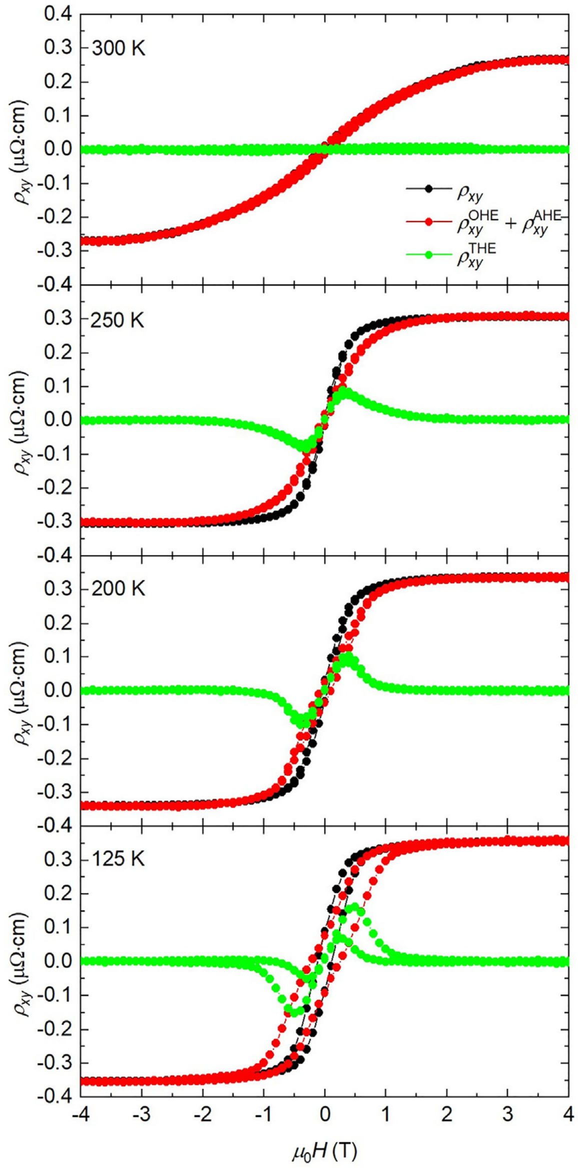

FIG. 4. Hall resistivities of 25 nm $NdCo_{4.4}Cu_{0.6}$ films under the out-of-plane magnetic field for the easy-axis ($T = 300\,K$, top panel), easy-cone (250 K, second), easy-plane (200 K, third), and biaxial *ab*-plane phases (125 K, bottom). Total resistivities ρ_{xy}, the sum of ordinary and anomalous Hall resistivities $\rho_{xy}^{OHE} + \rho_{xy}^{AHE}$, and topological Hall resistivities ρ_{xy}^{THE} are plotted by black, red, and green symbols, respectively.

and difficult to be identified from XRD measurements in Fig. 1(a). The phase mixture with Nd-rich crystals might affect low temperature transports there.

The temperature evolution of THE, measured every 25 K, is shown as the contour maps of ρ_{xy}^{THE} in Fig. 5. The results of positive field sweep directions from −4 to +4 T and from +4 to −4 T are shown in Figs. 5(a) and 5(b), respectively. A finite THE starts to appear when $\mathrm{NdCo_{4.4}Cu_{0.6}}$ shows the easy-cone phase below T_{SR2}. At this temperature range, ρ_{xy}^{THE} increases by decreasing temperature and takes the local maximum around the easy-plane phase at T_{SR1}. In the range of $T_{\mathrm{SR1'}} < T < T_{\mathrm{SR1}}$, the amplitude of THE remains almost constant as ρ_{xy}^{THE} ∼100 nΩ cm with negligible difference between two different field sweep directions. Moreover, the peak positions of $\rho_{xy}^{\mathrm{THE}}(H)$ remain consistent as $|H| = 0.3$–0.4 T by implying the EIPD to biskyrmion transitions at zero field vicinity, as observed in the direct imaging results in Ref. 20. These behaviors are distinctively changed at the biaxial *ab*-plane phase below $T_{\mathrm{SR1'}}$. The clear differences observed between field sweep directions indicate that the remanent THE after field switching [i.e., $H > 0$ in Fig. 5(a) or $H < 0$ in Fig. 5(b)] is notably larger. Further studies of micromagnetic and microstructure analyses will be required to discuss the details of THE origins at this temperature range.

In summary, we explored the magnetron sputtering fabrication of the $\mathrm{CaCu_5}$-type $\mathrm{NdCo_{5-x}Cu_x}$ thin films and observed a large THE at successive spin reorientations from the easy-plane, easy-cone, to easy-axis transitions. The obtained THE at $150\,\mathrm{K} < T \leq 250\,\mathrm{K}$ shows good consistency with the results of the early report on bulk $\mathrm{NdCo_5}$, indicating stabilization of spontaneous EIPD and/or skyrmion textures at zero field vicinity. The additional biaxial *ab*-plane MCA behavior appears below 150 K, associated with the nontrivial magnetic textures and transport properties at the lower temperature range. These observations of near-room temperature topological signals in thin films with the low-cost fabrication process will be an incremental step toward further development of spintronic devices using rare-earth intermetallics.

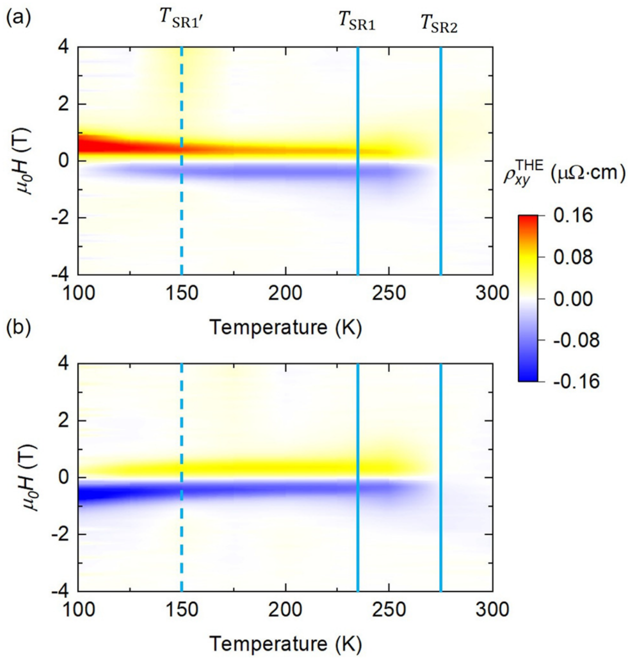

FIG. 5. Temperature and field evolutions of the topological Hall resistivity ρ_{xy}^{THE} of 25 nm $\mathrm{NdCo_{4.4}Cu_{0.6}}$ films for (a) the positive field direction from −4 to +4 T and (b) the negative field direction from +4 to −4 T. The spin reorientation temperatures $T_{\mathrm{SR1'}}$, T_{SR1}, and T_{SR2} are guided with blue lines.

This work was partially supported by the Japan Society for the Promotion of Science (JSPS) KAKENHI via Grant Nos. JP20K14419 and JST, PRESTO via Grant No. JPMJPR18L3, Japan.

AUTHOR DECLARATIONS

Conflict of Interest

The authors have no conflicts to disclose.

Author Contributions

Satoshi Sugimoto conceived the project, planned and performed experiments, and analyzed data. Satoshi Sugimoto, Y. K. Takahashi, and Shinya Kasai wrote the main text.

Satoshi Sugimoto: Conceptualization (lead); Data curation (lead); Formal analysis (lead); Funding acquisition (equal); Investigation (lead); Methodology (lead); Project administration (lead); Writing – original draft (lead); Writing – review & editing (lead). **Y. K. Takahashi:** Funding acquisition (equal); Project administration (equal); Writing – review & editing (equal). **Shinya Kasai:** Funding acquisition (equal); Project administration (equal); Resources (equal); Supervision (equal); Writing – review & editing (equal).

DATA AVAILABILITY

The data that support the findings of this study are available from the corresponding author upon reasonable request.

REFERENCES

[1] N. Nagaosa, J. Sinova, S. Onoda, A. H. MacDonald, and N. P. Ong, Rev. Mod. Phys. **82**, 1539 (2010).
[2] R. Karplus and J. M. Luttinger, Phys. Rev. **95**, 1154 (1954).
[3] J. Smit, Physica **24**, 39 (1958).
[4] L. Berger, Phys. Rev. B **2**, 4559 (1970).
[5] Z. Fang, N. Nagaosa, K. S. Takahashi, A. Asamitsu, R. Mathieu, T. Ogasawara, H. Yamada, M. Kawasaki, Y. Tokura, and K. Terakura, Science **302**, 92 (2003).
[6] J. Ye, Y. B. Kim, A. J. Millis, B. I. Shraiman, P. Majumdar, and Z. Tešanovic, Phys. Rev. Lett. **83**, 3737 (1999).
[7] P. Bruno, V. K. Dugaev, and M. Taillefumier, Phys. Rev. Lett. **93**, 096806 (2004).
[8] W. Wang, Y. Zhang, G. Xu, L. Peng, B. Ding, Y. Wang, Z. Hou, X. Zhang, X. Li, E. Liu, S. Wang, J. Cai, F. Wang, J. Li, F. Hu, G. Wu, B. Shen, and X. X. Zhang, Adv. Mater. **28**, 6887 (2016).
[9] Y. Gao, Q. Yin, Q. Wang, Z. Li, J. Cai, T. Zhao, H. Lei, S. Wang, Y. Zhang, and B. Shen, Adv. Mater. **32**, 2005228 (2020).
[10] A. Fert, V. Cros, and J. Sampaio, Nat. Nanotechnol. **8**, 152 (2013).
[11] A. Fert, N. Reyren, and V. Cros, Nat. Rev. Mater. **2**, 17031 (2017).
[12] A. Neubauer, C. Pfleiderer, B. Binz, A. Rosch, R. Ritz, P. G. Niklowitz, and P. Böni, Phys. Rev. Lett. **102**, 186602 (2009).
[13] N. Kanazawa, Y. Onose, T. Arima, D. Okuyama, K. Ohoyama, S. Wakimoto, K. Kakurai, S. Ishiwata, and Y. Tokura, Phys. Rev. Lett. **106**, 156603 (2011).

[14] S. Mühlbauer, B. Binz, F. Jonietz, C. Pfleiderer, A. Rosch, A. Neubauer, R. Georgii, and P. Böni, Science **323**, 915 (2009).
[15] X. Z. Yu, N. Kanazawa, Y. Onose, K. Kimoto, W. Z. Zhang, S. Ishiwata, Y. Matsui, and Y. Tokura, Nat. Mater. **10**, 106 (2011).
[16] K. Karube, J. S. White, N. Reynolds, J. L. Gavilano, H. Oike, A. Kikkawa, F. Kagawa, Y. Tokunaga, H. M. Ronnow, Y. Tokura, and Y. Taguchi, Nat. Mater. **15**, 1237 (2016).
[17] L. Peng, Y. Zhang, W. Wang, M. He, L. Li, B. Ding, J. Li, Y. Sun, X. G. Zhang, J. Cai, S. Wang, G. Wu, and B. Shen, Nano Lett. **17**, 7075 (2017).
[18] F. Zheng, H. Li, S. Wang, D. Song, C. Jin, W. Wei, A. Kovacs, J. Zang, M. Tian, Y. Zhang, H. Du, and R. E. D. Borkowski, Phys. Rev. Lett. **119**, 197205 (2017).
[19] F. Tejo, D. Toneto, S. Oyarzun, J. Hermosilla, C. S. Danna, J. L. Palma, R. B. da Silva, L. S. Dorneles, and J. C. Denardin, ACS Appl. Mater. Interfaces **12**, 53454 (2020).
[20] S. Zuo, J. Liu, K. Qiao, Y. Zhang, J. Chen, N. Su, Y. Liu, J. Cao, T. Zhao, J. Wang, F. Hu, J. Sun, C. Jiang, and B. Shen, Adv. Mater. **33**, 2103751 (2021).
[21] C. Patterson, D. Givers, J. Voiron, and S. B. Palmer, J. Magn. Magn. Mater. **54–57**, 891 (1986).
[22] P. A. Algarabel, A. del Moral, M. R. Ibarra, J. B. Sousa, J. M. Moreira, and J. F. Montenegro, J. Magn. Magn. Mater. **68**, 177 (1987).
[23] K.-W. Moon, J. Yoon, C. Kim, and C. Hwang, Phys. Rev. Appl. **12**, 064054 (2019).
[24] Z. J. Guo, J. S. Jiang, J. E. Pearson, S. D. Bader, and J. P. Liu, Appl. Phys. Lett. **81**(11), 2029 (2002).
[25] S. R. Jones, A. Dunhill, R. A. Cowley, and R. C. C. Ward, Phys. Rev. B **77**, 214110 (2008).
[26] R. Cid, G. R. Rodríguez, L. M. Álvarez-Prado, J. Díaz, and J. M. Alameda, J. Magn. Magn. Mater. **316**, e446 (2007).
[27] J. Díaz, R. Cid, A. Hierro, L. M. Álvarez-Prado, C. Quirós, and J. M. Alameda, J. Phys.: Condens. Matter **25**, 426002 (2013).
[28] M. Seifert, L. Schultz, and V. Neu, J. Appl. Phys. **106**, 073915 (2009).
[29] M. Seifert, L. Schultz, and V. Neu, J. Appl. Phys. **107**, 09A711 (2010).
[30] Y. C. Chuang, C. H. Wu, and J. Fong, J. Less-Common Met. **133**, 215 (1987).
[31] T. Miyasato, N. Abe, T. Fujii, A. Asamitsu, S. Onoda, Y. Onose, N. Nagaosa, and Y. Tokura, Phys. Rev. Lett. **99**, 086602 (2007).
[32] X. Z. Yu, Y. Tokunaga, Y. Kaneko, W. Z. Zhang, K. Kimoto, Y. Matsui, Y. Taguchi, and Y. Tokura, Nat. Commun. **5**, 3198 (2014).
[33] J. Sampaio, V. Cros, S. Rohart, A. Thiaville, and A. Fert, Nat. Nanotechnol. **8**, 839 (2013).
[34] R. Tomasello, E. Martinez, R. Zivieri, L. Torres, M. Carpentieri, and G. Finocchio, Sci. Rep. **4**, 6784 (2014).
[35] K. Y. Guslienko, V. Novosad, Y. Otani, H. Shima, and K. Fukamichi, Phys. Rev. B **65**, 024414 (2001).
[36] G. Yu, A. Jenkins, X. Ma, S. A. Razavi, C. He, G. Yin, Q. Shao, Q. l He, H. Wu, W. Li, W. Jiang, X. Han, X. Li, A. Claire, B. Jayich, P. K. Amiri, and K. L. Wang, Nano Lett. **18**(2), 980 (2018).
[37] M. He, L. Peng, Z. Zhu, G. Li, J. Cai, J. Li, H. Wei, L. Gu, S. Wang, T. Zhao, B. Shen, and Y. Zhang, Appl. Phys. Lett. **111**, 202403 (2017).
[38] C. H. Wu, Y. C. Chuang, X. M. Jin, and X. H. Guan, Z. Metallkd **83**, 162 (1992).